Cryostratigraphy and the sublimation unconformity in permafrost from an ultraxerous environment, University Valley, McMurdo Dry Valleys of Antarctica.

Caitlin M. Lapalme[1], Denis Lacelle[1], Wayne Pollard[2], Daniel Fortier[3], Alfonso Davila[4], Christopher P. McKay[4]

[1]Department of Geography, Environment and Geomatics, University of Ottawa, Ottawa, ON, Canada
[2]Department of Geography, McGill University, Montreal, QC, Canada
[3]Département de Géographie, Université de Montréal, Montréal, QC, Canada
[4]NASA Ames Research Center, Moffet Field, CA, USA
*Corresponding author: D. Lacelle (dlacelle@uottawa.ca)

Permafrost and Periglacial Processes – accepted March 24th, 2017

Abstract. The cryostratigraphy of permafrost in ultraxerous environments is poorly known. In this study, icy permafrost cores from University Valley (McMurdo Dry Valleys, Antarctica) were analyzed for sediment properties, ground-ice content, types and distribution of cryostructures and presence of unconformities. No active layer exists in the valley, but the ice table, a sublimation unconformity, ranges from 0 to 60 cm depth. The sediments are characterized as a medium sand, which classifies them as low to non-frost susceptible. CT scan images of the icy permafrost cores revealed composite cryostructures that included the structureless, porous visible, suspended and crustal types. These cryostructures were observed irrespective of ground-ice origin (vapour deposited and freezing of snow meltwater), suggesting that the type and distribution of cryostructures could not be used as a proxy to infer the mode of emplacement of ground ice. Volumetric ice content derived from the CT scan images under-estimated measured volumetric ice content, but approached measured excess ice content. A paleo-sublimation unconformity could not be detected from a change in cryostructures, but could be inferred from an increase in ice content at the maximum predicted ice table depth. This study highlights some of the unique ground ice processes and cryostructures in ultraxerous environments. **Keywords:** cryostratigraphy, sublimation unconformity, ground ice, permafrost, CT scan, McMurdo Dry Valleys of Antarctica

INTRODUCTION

Cryostratigraphy is an approach that emphasizes the description of cryostructures (distribution and shape of ground ice in permafrost), the quantification of ground-ice content and associated cryofacies, and the identification of unconformities in permafrost. Together, the elements of the cryostratigraphic approach help determine the nature of ground-ice emplacement and the history of permafrost (e.g. French, 1998; French and Shur, 2010; Gilbert *et al*., 2016). Cryostratigraphic studies have focused on Arctic permafrost, where permafrost soils are moist to water-saturated, the principle moisture source is liquid water, the main mechanism of ground-ice formation is freezing of water, and unconformities relate to the thaw of near-surface permafrost during past warmer periods (i.e. thaw unconformities) (Mackay, 1972; Fortier *et al*., 2008; French and Shur, 2010; Douglas *et al*., 2011; Gilbert *et al*., 2016). Little is known about the application of cryostratigraphy in permafrost from ultraxerous environments, such as the high-elevation terrain in Antarctica, where the principle moisture source is vapour and the main mechanism of ground-ice formation is vapour deposition. In these regions, the permafrost table is at or near the ground surface (Adlam *et al*., 2010); however, the position of the ice table, which is the interface between dry and ice-bearing permafrost, reflects the equilibrium depth between seasonal vapour deposition and sublimation (Fisher *et al*., 2016). The ice table therefore represents a sublimation unconformity, in a similar manner as the permafrost table represents a thaw unconformity.

In University Valley, situated in the upper McMurdo Dry Valleys (MDV) of Antarctica, icy permafrost was found below a shallow ice table (McKay, 2009; Marinova *et al*., 2013). Based on its δD-$\delta^{18}O$ composition, the ground ice in the sandy sediments was emplaced by three different mechanisms: vapour deposition, freezing of partially evaporated snow meltwater and burial of glacier ice (Lacelle *et al*., 2011, 2013; Pollard *et al*., 2012; Lapalme *et al*., 2017). The differing ground-ice emplacement processes in University Valley allow us to assess the application of cryostratigraphy in an ultraxerous region and its ability to help infer the origin of ground ice and the past permafrost conditions (i.e. the presence of a paleo-sublimation unconformity). Using ice-bearing permafrost cores collected from University Valley, the objectives of this study are to: (1) describe cryostructures in the permafrost cores, based on computed tomography (CT) scan images, to determine if differing ground-ice origins generate distinct cryostructures; (2) determine the potential presence of sublimation unconformities in the icy permafrost; and (3)

derive volumetric ice contents in permafrost using the CT scan images and compare the results with measured volumetric and excess ice contents. Overall, this study highlights some of the unique ground-ice processes in ultraxerous environments, where the availability of moisture is limited.

STUDY AREA

University Valley is 1.5 km long and situated in the Quartermain Mountains of the MDV, Antarctica (77°52'S, 163°45'E), 1600-1800 m above sea level (a.s.l.) (Figure 1). A small glacier is situated at the head of the valley and permanent snow patches are found in depressions located in the western portion of the valley floor. Sand-wedge polygons, typical of ultraxerous environments (Marchant and Head, 2007), occupy the valley floor and some of the talus cones. Polygon diameters range from ca. 10 m in the upper section of the valley to ca. 20 m in the lower section (Mellon et *al.,* 2014).

The local bedrock consists of Jurassic age sills of Ferrar Dolerite and Devonian to Triassic age sandstones and conglomerates of the Beacon Supergroup (Barrett, 1981; Cox *et al.,* 2012). The surficial sediments comprise alpine drift in the upper and middle regions of the valley, undifferentiated till in the lower part, and colluvium and talus cones at the base of valley walls (Cox *et al.,* 2012). Optically-stimulated luminescence ages obtained from permafrost cores from four polygons in upper and middle University Valley (P1, P2, P8, P12) yielded ages of 17.9 ± 1.6 kyr for sediments at 2-5 cm depths, whereas those at 90-95 cm depths were dated to 170 ± 36 kyr (Lacelle *et al.,* 2013; Trinh-Le, 2017). These ages fit reasonably well with those derived from Cl accumulation in the upper 56 cm of sediments (Jackson *et al*., 2016). The undifferentiated till, which contains granite erratics, is likely associated with the Taylor 4b Drift (>2.7 Ma) or an older glaciation (Cox *et al.,* 2012; Dickinson *et al*., 2017). Given the apparent continuous sediment accumulation of the alpine drift over the last 200 ka and enduring cold-climate conditions for the last 12 Ma (Lewis *et al.,* 2007, 2008), the permafrost in the sediments along the valley floor is likely syngenetic.

University Valley is situated in the stable upland climate zone of the MDV, a region characterized by summer air temperatures <0°C, relative humidity values near 50% (Doran *et al*., 2002; Marchant and Head, 2007) and low precipitation (<10 mm snow water equivalent; Fountain *et al*., 2009). Three years of climate data (2010-2012) collected from an automated

weather station in University Valley indicated a mean annual air temperature of –23.4 ± 0.9°C, a mean annual relative humidity of 45.5 ± 1.8% and maximum hourly air temperatures always <0°C (Lacelle *et al*., 2016). Two distinct ground-surface temperature zones have been identified in the valley (Figure 1e): (1) a perennially cryotic zone (PCZ) in the north-east section of the valley, characterized by ground-surface temperatures always <0°C; and (2) a seasonally non-cryotic zone (NCZ), characterized by ground-surface temperatures that rise above 0°C for at least a few hours on clear summer days. The transitional area between the PCZ and NCZ is referred to as the intermediate mixed zone (IMZ) and may exhibit characteristics of either zone.

The permafrost table along the floor of University Valley is at the ground surface (Lacelle *et al*., 2016), whereas the ice table ranges in depth from 0 cm near the glacier to ca. 60 cm at the mouth of the valley (McKay, 2009; Marinova *et al*., 2013). Fisher *et al*. (2016) concluded that the measured ice-table depths are likely in equilibrium with present-day ground-surface temperature and humidity conditions. Ground ice is abundant below the ice table, with excess ice contents, excluding the two buried glacier-ice bodies, reaching 93% (Lapalme *et al*., 2017). Based on δD-δ^{18}O measurements, ground ice has been attributed to three different origins: (1) vapour deposition in the sediments from the PCZ; (2) freezing of partially evaporated snow meltwater in the sediments from the NCZ; and (3) buried glacier ice at two localities (Lacelle *et al*., 2011, 2013; Pollard *et al*., 2012; Lapalme *et al*., 2017).

METHODOLOGIES

Field sampling and core selection

Between 2009 and 2013, 18 ice-bearing permafrost cores were collected using an 11.5 cm diameter SIPRE corer from 12 polygons along the length of the valley (Figure 1). Prior to coring, the dry sediment layer above the ice-bearing permafrost was removed. Each core was retrieved in 10 to 50 cm long segments, wrapped in plastic core sleeves and shipped frozen in thermally insulted boxes to the University of Ottawa (Ottawa, Canada).

All cores were analyzed for ground-ice content and five were imaged using CT scanning (P1-C1, P6-C5, P7-C1, P8-C3 and P8-C6). These cores were selected because of their location in the valley with respect to the ground-surface temperature zones and ground-ice origins. P8 and P6 are situated in the PCZ and the IMZ, respectively, where the ground ice in the cores was

attributed to vapour deposition, whereas P1 and P7 are situated in the NCZ, where the ground ice formed by the freezing of partially evaporated snowmelt water (Lapalme *et al*., 2017).

CT scanning and image processing

The top section of the permafrost cores were scanned using a Siemens Somaton Volume Access dual CT scanner (pixel resolution of 0.4 mm for x, y and z axes) at the Institut National de la Recherche Scientifique (Québec, Canada). The technique produces a series of cross-section image slices that represent the relative X-ray absorption rate, from which the CT value in Hounsfield Units (HU) can be calculated (Hounsfield, 1973; Kawamura, 1990). Density was calculated relative to that of water; thus, water has a value of 0 HU and air has values near –1000 HU (Kawamura, 1990; Delisle *et al*., 2003). When combined into an image stack, the image slices create a grey-scale image representing a 3D reconstruction of the density variations of the materials in the cores. Darker tones indicate lower density materials (i.e. gas and ice), and lighter tones indicate higher density material (i.e. sediments) (e.g. Hounsfield, 1973; Calmels and Allard, 2004, 2008; Torrance *et al*., 2008). Image processing and interpretations of the CT scan images depend on the threshold values determined for the various components of the core. The threshold value for identifying ice in the permafrost cores (–320 to 775 HU) was determined through analyzing the histograms of density measurements in the image stacks (e.g. Dillon *et al*., 2008; Obbard *et al*., 2009; Calmels *et al*., 2012).

Classification of cryostructures using CT scan images

Cryostructures are defined as the description of the distribution and shape of ground ice in permafrost (Murton and French, 1994). CT scan images reveal cryostructures in a permafrost core at the millimeter scale, resulting in a more detailed description than would otherwise be possible along natural permafrost exposures or upon retrieval of permafrost cores (e.g. Shur *et al*., 2004; Kanevskiy *et al*., 2011, 2013, 2014). The cryostructures visible in the CT scan images were identified using the Murton and French (1994) classification, which includes lenticular, suspended, reticulate, layered, structureless and crustal cryostructures, with the addition of porous visible cryostructure, defined as random inclusions of ice that fill large pores (i.e. Stephani *et al*., 2010; Kanevskiy *et al*., 2011, 2013). Cryostructures were analyzed using the *Orthogonal Views* function in *Fiji* image analysis software.

Ground-ice content derived from analysis of CT scan images

Volumetric ice content was calculated from each slice (0.4 mm resolution) of the CT scan images (VIC_{CT}) using the –320 to 750 HU threshold for ice and the *Analyze Particles* function in *Fiji* image analysis software. Using other thresholds (–200 to 700, –200 to 750, –250 to 700, –250 to 750) had little effect on the calculated VIC_{CT} of the cores (Lapalme *et al*., 2015). The resulting *masks* from the function represent the filled outlines of the measured particles that were used to compute the total area covered by the particles (Ferreira and Rasband, 2012). The slices in the image stacks corresponding to breaks in the core segments and/or where the core image was smaller than the region of interest were removed as these slices would misrepresent the ice content in the core. To assess the accuracy of the volumetric ice content derived from the CT scan images, the VIC_{CT} values were correlated with measured volumetric and excess ice contents.

Calculation of ground-ice content and accumulation rates

Following CT scan imaging, the permafrost cores were cut into ca. 2 cm thick slices and thawed in sealed plastic bags. Once thawed, the cores were transferred into graduated 50 ml polypropylene tubes, where the sediments settled. The volume of supernatant water (if present) and sediments were recorded. Excess ice content (EIC), defined as the volume of ice in the ground exceeding the total pore volume that the ground would have under natural unfrozen conditions (van Everdingen, 1998), was calculated as:

$$EIC\ (\%) = \frac{Ws \times 1.0917}{(Ws \times 1.0917 + Vs)} \times 100 \qquad (1)$$

where Ws is the volume of supernatant water (cm^3), Vs is the volume of sediments (cm^3) and the number 1.0917 is used to convert the measured volume of supernatant water to the equivalent volume of ice.

The volumetric ice content (VIC), defined as the volume of ice per unit volume of icy soils (van Everdingen, 1998), was determined as:

$$VIC\ (\%) = \frac{\mathrm{Wv} \times 1.0917}{Vt} \times 100 \qquad (2)$$

where Wv is the volume of the water in the sample (cm^3), Vt is the total volume of the sample (cm^3) determined from the core sample dimension. Wv is derived from the total mass of water in the sample (g), assuming a water density of 1.0 g cm^3.

Based on the VIC values, cryofacies types were defined as: pure ice (100% VIC), sediment-poor ice (>75% VIC), sediment-rich ice (>50 to ≤75% VIC), ice-rich sediment (>25 to ≤50% VIC) or ice-poor sediment (≤25% VIC) (Murton and French, 1994).

Apparent rates of ground-ice accumulation in the icy permafrost were calculated by dividing the cumulative volume of water in the core by the surface area of core barrel and by age of the soils, estimated from optically-stimulated luminescence ages and Cl concentrations (Lacelle *et al*., 2013; Jackson *et al.,* 2016). Since Cl-derived ages were obtained for the top 56 cm of soils, the cumulative volume of water was calculated to this depth for sites with cores equal or longer than 56 cm (i.e., three cores discussed in this paper: P8-C3, P6-C5 and P1-C1; and three sites discussed in Lapalme *et al.,* 2017: P12, P1-C2 and P6-C3).

Determination of sediment properties

The grain-size distribution of the sediments was determined at ca. 10 cm depth intervals using the stacked sieve method (2, 1, 0.5, 0.25, 0.125 and 0.0625 mm) and classified into three dominant particle sizes: gravel (≥2 mm), sand (<2 mm to ≥0.0625 mm), and silt and clay (<0.0625 mm). Two representative soil samples from P8-C3 and P1-C1 were analyzed by mercury porosimetry to determine their porosity and pore-size distribution (analysis performed by Micromeritics Analytical Services, Norcross GA, USA).

RESULTS

Sediment properties

The sediment in the five cores is a pale brown (10YR 6/3) medium sand (0.25 to 0.5 mm), with <8% silt and clay (Figure 2). In each core, the grain-size distribution changed little with depth. In the three permafrost cores from the PCZ and IMZ (P8-C6, P8-C3, P6-C5), sand-sized particles ranged from 47 to 96%, gravel between 1 and 52%, and silt and clay occupied <5%. In the two permafrost cores from the NCZ (P7-C1 and P1-C1), the values were 76–97% sand, 0.3–21% gravel and <8% silt and clay. According to Andersland and Ladanyi (2004), the sediments in the icy permafrost cores can be classified as low to non-frost susceptible.

Given the homogenous grain-size distribution, mercury porosimetry was performed on two samples. The porosity of P8-C3 and P1-C1 was 28 and 37%, respectively. The pore-space diameter of both sandy sediment samples ranged from 4 μm to 0.3 mm, with a unimodal distribution (dominant mode at 0.1 mm; Figure 2c). These porosities and pore-space distributions are similar to those determined in sandy sediments elsewhere in the upper MDV, such as Beacon Valley and Linneaus Terrace (Sizemore and Mellon, 2008).

Cryostructures and discontinuities

The CT scan images revealed multiple types of cryostructures across the same depth interval, including structureless, porous visible, suspended and crustal (Figure 3). All the observed cryostructures were composite in nature (Figure 4). The structureless, porous visible and crustal cryostructures were identified at all depths in the five permafrost cores. The suspended cryostructure was observed in all cores except P8-C6. The shape and size of the suspended cryostructure varied between the cores; those in P7-C1 and P1-C1 were predominantly smaller than those in P6-C5 and P8-C3. No trend in the distribution of the crustal cryostructures was discernable in the five cores as the ice rims, typically a few mm thick, either: (1) fully surrounded the sand or gravel particles; (2) covered or partially covered one side of them; or (3) contained a combination of both scenarios. The crustal cryostructures were more difficult to distinguish in P1-C1 as the gravel content was low at most of the investigated depths, resulting in much smaller sediment grains around which the ice rims developed. With the exception of the P8-C6 core, the relative proportion of individual cryostructures within the composite cryostructure varied with depth within each core as a reflection of the presence or absence of the suspended cryostructure. No unconformity in the form of a change in cryostructures with depth could be detected.

Ground-ice content and accumulation rates

In the five icy permafrost cores, EIC and VIC ranged from 0 to 66% and 32 to 82%, respectively, with both measurements being highly correlated (Figure 5). In P8-C3, collected in the center of a polygon in the PCZ, a shallow ice-rich horizon was observed just below the ice table. This ice-rich layer was not present in the shoulders of the polygons in the PCZ and IMZ (P8-C6, P6-C5). In all polygons in the PCZ, ground-ice content increased at ca. 40-50 cm below

the ground surface, resulting in an ice-rich zone in the uppermost 40-80 cm. In the NCZ, the two cores did not display the shallow ice-rich layer; however, like those in the PCZ the ground-ice content increased abruptly at ca. 40-50 cm below the surface. Figure 5 also shows the VIC_{CT} in the five permafrost cores. VIC_{CT} values were consistently lower than VIC, although the distribution of VIC_{CT} with depth more closely followed that of EIC. Using a linear regression analysis (Figure 6), the relation between VIC_{CT} values averaged over the same depth intervals as VIC and EIC (ca. 2 to 3 cm) showed a positive linear relation, but VIC_{CT} under-estimated VIC (VIC_{CT} (%) = 0.75 VIC (%) + 36.52; $r^2 = 0.45$; $p = <0.05$), while VIC_{CT} and EIC showed a better correlation, apporaching the 1:1 line (VIC_{CT} (%) = 0.79 EIC (%) + 1.32; $r^2 = 0.67$, $p = <0.05$).

Based on the ground-ice content and age of the sediments, apparent rates of ice accumulation were calculated to infer moisture availability and transfer rates between the colder PCZ and warmer NCZ (Figure 7). Apparent ice accumulation rates in the PCZ ranged from 6.9 x 10^{-4} mm yr^{-1} to 1.15 x10^{-2} mm yr^{-1}. This range is similar to those calculated using the REGO vapour diffusion and deposition model (Lacelle *et al*., 2013; Fisher and Lacelle, 2014; Fisher *et al*., 2016). Apparent ice accumulation rates for sites in the NCZ yielded values in the same range, indicating similar moisture transfer rates in the differing thermal regions of the valley.

DISCUSSION

Previous cryostratigraphic studies of permafrost have focussed on (1) permafrost soils that were moist to water-saturated; (2) ground ice formed mainly from freezing of liquid water; and (3) discontinuities in the form of thaw unconformities (e.g. French and Shur, 2010; Gilbert *et al*., 2016). Here we discuss the cryostratigraphy of permafrost in University Valley where: (1) the sediments in which syngenetic permafrost aggraded were dry to nearly dry; (2) the principle moisture sources were vapour and snow meltwater; (3) the main mechanisms of ground-ice formation were vapour-deposition and freezing; and (4) discontinuities are in the form of sublimation unconformities.

Cryostructures in low frost-susceptible sediments of ultraxerous environments

In the low frost-susceptible sediments of University Valley, four types of cryostructures were observed, including: structureless, porous visible, suspended and crustal, irrespective of their location in the valley (PCZ, NCZ or IMZ) and the associated origin of ground ice: vapour-

deposited ground ice in the PCZ and freezing of partially evaporated snow meltwater in the NCZ (Lacelle *et al*., 2013; Lapalme *et al*., 2017). Therefore, the type of cryostructure observed in the cores could not be used to infer the mode of emplacement of ground ice.

The similar cryostructures, ground-ice content and ice accumulation rates in the University Valley icy permafrost cores, irrespective of ground-ice origin, suggest that the cryostructures represent a transition from structureless to suspended as ice accumulates in the sediments. This process would depend on soil texture and the amount of available moisture in the icy cold permafrost (Figure 8). Optically-stimulated luminescence age from four sites in University Valley showed that sediments in the uppermost 1 m have been accreting for at least the last 170 ka (Lacelle *et al.,* 2013; Trihn-Lee, 2017). If we begin with dry sandy sediments with a porosity (n) that is subsequently filled with ice, the maximum content of pore ice would be:

$$Pore\ ice_{max}(g\ g^{-1}\ dry\ sediments) = \frac{0.917n}{\rho} \qquad (3)$$

where ρ is the dry bulk density of the sediments.

For typical University Valley sediments with ρ = 1.3 g cm^{-3} and n = 0.33, the maximum pore-ice content would be 0.23 g g^{-1} dry sediments. At this stage, the pore-ice conditions in the sandy sediments would be represented by a structureless cryostructure in smaller pore spaces and a porous visible cryostructure in larger ones. A crustal cryostructure could also be present at this stage as ice could grow around gravel clasts and smaller sand particles; albeit, the ice crust may not fully surround them yet at this stage. In University Valley, modelling estimates have shown that it would take ca. 225 years to fill the pore space of the sediments with ice by vapour deposition (Lacelle *et al*., 2013). Given the similar apparent ice-accumulation rate between the PCZ and NCZ, we estimate that it would take a comparable time to fill dry sediments with partially evaporated snow meltwater. But this process that would not necessarily occur each summer in view of the low snow recurrence interval (McKay, 2009).

The presence of the suspended cryostructure in the icy permafrost of University Valley is frequently associated with EIC values >10% (Figure 5). The development of the suspended cryostructure is likely caused by the downward propagation of daily and seasonal temperature waves, setting up tensile stress in mixtures of pore ice and sediments (Mellon, 1997; Fisher, 2005; Fisher *et al*., 2016). This in turn generates voids and cracks induced by the difference in the thermal contraction and expansion coefficients of ice and rock, with that of ice being about 10 times that of most rocks (Fisher, 2005; Fisher *et al*., 2016). During each temperature cycle,

voids and cracks of various sizes generated in the icy sediments increase the available pore space to the depth of zero daily and annual temperature amplitudes, and become partially filled with new ice (either from vapor deposition or freezing of partially evaporated snowmelt). Because the cracks do not close to their original configuration after each thermal contraction cycle, this results in a progressive net increase of ice content above the initial porosity of the sediments, forming the observed suspended cryostructure, and heaving the overlying sediment. The progressive accumulation of ground ice, beginning from dry sediments that subsequently fill with pore ice and eventually reach excess ice contents ca. 80%, would take ca. 10,000 years in this ultraxerous environment (Lacelle *et al*., 2013).

Overall, our results indicate that the structureless, porous visible, suspended and crustal cryostructures can form by both vapour deposition and the freezing of infiltrating snow meltwater in sandy cryotic sediments. The observation of these cryostructures in low frost-susceptible sediments may therefore not be diagnostic of the moisture source or transfer process related to their development, particularly in ultraxerous environments. This finding challenges the current genetic classification of cryogenic structures that attributed the formation of these cryostructures to the freezing of moisture through cryosuction and other liquid water movement mechanisms in soils (i.e. Murton and French, 1994; French and Shur, 2010). The discrepancy between findings likely results from the very low ice-accumulation rate in the low frost-susceptible sediments of University Valley (in the order of 10^{-4} to 10^{-2} mm yr^{-2}). This highlights the importance of availability of moisture and its transfer rate to grow ground ice and the associated development of cryostructures in ultraxerous environments where the sediments are deposited dry to nearly dry and permafrost is syngenetic.

Cryostratigraphy and the sublimation unconformity in ultraxerous environments

The cryostratigraphic approach is commonly used to identify unconformities in permafrost where these are evidenced by a change in the distribution of cryostructures and ground-ice content (e.g. French and Shur, 2010; Gilbert *et al*., 2016). Unconformities in permafrost have previously been identified as thaw unconformities and attributed to a deeper thaw of permafrost under past warmer climate conditions and subsequent permafrost re-aggradation (e.g. Burn 1997; Fortier *et al.,* 2008). In University Valley and other areas in the upper MDV, the permafrost table is at or near the ground surface; however, the position of the ice table reflects the equilibrium

depth between seasonal vapour deposition and sublimation (Fisher *et al*., 2016). Characteristically comparable to the permafrost table, the ice table is likely temporally dynamic and its depth will vary following temperature and humidity changes at the ground surface (Figure 9). According to Fisher *et al*. (2016), the maximum ice-table depth for medium-grained sand, like that of University Valley, is expected to reach ca. 50 cm when ground-surface relative humidity ranges from 50 to 60%$_{ice}$.

In the five icy permafrost cores, no change in the type and distribution of cryostructures was observed in the uppermost 1 m (Figure 5). However, a paleo-sublimation unconformity could potentially be inferred from the abrupt increase in ice content at ca. 40-60 cm, which corresponds to the maximum predicted ice-table depth (Figure 5). The ground ice in the uppermost ca. 50 cm of the sediment column can accumulate and sublimate following changes in ground surface temperature and humidity conditions, although sublimation would be at a slower rate due to pore ice impeding vapour fluxes. However, the ground ice below 50 cm depth would continuously accumulate ice at a rate of ca. 0.03 kg m^{-2} yr^{-1} (Fisher *et al*., 2016), progressively increasing ice content over time. Therefore, unlike paleo-thaw unconformities, which can be identified by a change in the distribution of cryostructures, it does not appear that paleo-sublimation unconformities can be identified using the same approach.

Deriving ground ice content from CT scan images

Previous studies inferred that VIC$_{CT}$ could be used to estimate the ground-ice content of permafrost (Delisle *et al*., 2003; Calmels and Allard, 2004, 2008; Calmels *et al*., 2008). The studies were based on frost-susceptible soils that host thick ice lenses or bodies of massive ground ice, and VIC$_{CT}$ was not correlated with measured ground-ice contents. Here, we assessed the accuracy of VIC$_{CT}$ to predict ground-ice contents in the low frost-susceptible sediments of University Valley. Linear regression analysis revealed that VIC$_{CT}$ under-estimated measured VIC, but VIC$_{CT}$ and measured EIC showed a better correlation, apporaching the 1:1 line (Figure 6). This is attributed to the pixel resolution of the scan images (0.4 mm) and the relation between porosity and the distribution of pore-space diameter of the sediments, namely the fraction of pore-space diameter being lower than the pixel resolution. For example, pore ice in the medium-grained sand with an average porosity of 33% and a maximum pore space diameter of 0.3 mm (Figure 3) is not spatially resolvable in CT scan images with a pixel resolution of 0.4 mm.

However, EIC in these sediments can be estimated more accurately with VIC_{CT}, especially when the dimension of the ice component exceeds the pixel resolution of the CT scan images.

Overall, VIC_{CT} has the potential to estimate the distribution and abundance of ground ice. However, the accuracy of VIC_{CT} would depend on: (1) the relation between porosity and the distribution of pore-space diameter of the sediments; and (2) the type of instrument used for CT scanning and its associated pixel resolution. For clay and silt, which tend to have high porosities (>50%; Head, 1992) and pore-space diameters less than the CT scan image resolution, VIC_{CT} would not be able to detect pore ice, but should be able to detect ice lenses if their dimensions exceed 0.8 mm (due to mixed pixel effect, the detection of an object being analyzed likely has to be greater than twice the pixel resolution; Jensen, 2002). For sand, which tends to have porosities near 30-50% (Head, 1992) and pore-space diameters that approach the resolution of the CT scan image, VIC_{CT} would estimate EIC reasonably but underestimate VIC as some pore ice would not be spatially resolvable. For coarse sand and gravel, with porosities typically less than 30% (Head, 1992) and pore-space diameters that exceed the image resolution, VIC_{CT} should provide a reasonable estimate of VIC given that interstitial ice could be spatially resolved. As such, the relationship between VIC, EIC and VIC_{CT} illustrated in Figure 6 should not be applied to all sediment types; future studies would need to quantify the relation between VIC and VIC_{CT} to correct, if necessary, VIC_{CT} for other sediment types.

CONCLUSIONS

Based on the analyses of sediment properties, ground-ice content and CT scan images of icy permafrost cores from University Valley, Antarctica, the following conclusions can be made:

1) Sediments in the valley were characterized by a medium sand texture, with low fine-grained content, which classifies them as low to non-frost susceptible. However, the sediments still contained abundant ground ice, with excess ice and volumetric ice contents that reached 66% and 82%, respectively.
2) Volumetric ice content derived from the CT scan images of the permafrost cores under-estimated measured volumetric ice content, but approached the excess ice content due to the pixel resolution of the CT scan images, and the relation between porosity and the distribution of pore space diameter of the sediments.

3) Analysis of CT scan images of the permafrost cores revealed composite cryostructures that included the structureless, porous visible, suspended and crustal types. These cryostructures were observed irrespective of ground-ice origin (vapour deposited or freezing of snowmelt). Hence, the type and distribution of cryostructures may not be a proxy for the mode of emplacement of ground ice in low frost-susceptible sediments in ultraxerous environments.
4) In the ultraxerous environment of University Valley the permafrost table is at or near the surface, and thaw unconformities have not been observed. However, the ice table, which can be represented as a sublimation unconformity, typically appears in the uppermost 60 cm of permafrost. A paleo-sublimation unconformity could not be detected from a change in cryostructure, but could be inferred from a conspicuous increase in ice content at ~40-60 cm depth, which corresponds to the maximum predicted ice table depth in the valley.

ACKNOWLEDGEMENTS

Fieldwork in University Valley was supported by NASA's ASTEP grant to C.P. McKay and operated by the National Science Foundation Office of Polar Programs. NSERC Discovery grants to D. Lacelle, D. Fortier and W. Pollard provided financial support for laboratory analyses. We thank the two reviewers and editor for their constructive comments on the manuscript.

REFERENCES

Adlam LS, Balks MR, Seybold CA, Campbell DI. 2010. Temporal and spatial variation in active layer depth in the McMurdo Sound Region, Antarctica. *Antarctic Science* **22**: 45-53. DOI:10.1017/S0954102009990460

Andersland OB, Ladanyi B. 2004. *Frozen Ground Engineering*, Second Edition. John Wiley and Sons: Chichester

Barrett PJ. 1981. History of the Ross Sea region during the deposition of the Beacon Supergroup 400–180 million years ago. *Journal of the Royal Society of New Zealand* **11**: 447–458. DOI:10.1080/03036758.1981.10423334

Burn C. 1997. Cryostratigraphy, paleogeography, and climate change during the early Holocene warm interval, western Arctic coast, Canada. *Canadian Journal of Earth Sciences* **34**: 912-925. DOI:10.1139/e17-076

Calmels F, Allard M. 2004. Ice segregation and gas distribution in permafrost using tomodensitometric analysis. *Permafrost and Periglacial Processes* **15**: 367-378. DOI: 10.1002/ppp.508

Calmels F, Allard M. 2008. Segregated ice structures in various heaved permafrost landforms through CT scan. *Earth Surface Processes and Landforms* **33**: 209-225. DOI: 10.1002/esp.1538

Calmels F, Delisle G, Allard M. 2008. Internal structure and the thermal and hydrological regime of a typical lithalsa: significance of permafrost growth and decay. *Canadian Journal of Earth Sciences* **45**: 31-43. DOI: 10.1139/E07-068

Calmels F, Froese DG, Clavano WR. 2012. Cryostratigraphic record of permafrost degradation and recovery following historic (1898-1992) surface disturbances in the Klondike region, central Yukon Territory. 2012. *Canadian Journal of Earth Sciences* **49**: 938-952. DOI: 10.1139/e2012-023

Cox SC, Turnbull IM, Isaac MJ, Townsend DB, Smith BL. 2012. Geology of southern Victoria Land Antarctica. Institute of Geological and Nuclear Sciences, Geological Map 22. GNS Science: Lower Hutt, New Zealand.

Delisle G, Allard M, Fortier R, Calmels F, Larrivée E. 2003. Umiujaq, Northern Québec: innovative techniques to monitor the decay of a lithalsa in response to climate change. *Permafrost and Periglacial Processes* **14**: 375-385. DOI: 10.1002/ppp.469

Dickinson WW, Williams G, Hill M, Cox SC, Baker JA. 2017. Granite erratics in Beacon Valley, Antarctica. Antarctic Science. DOI:10.1017/S0954102017000013

Dillon M, Fortier, D, Kanevskiy M, Shur Y. 2008. Tomodensitometric analysis of basal ice. In *9th International Conference on Permafrost*, *June 28 – July 3 2008, Proceedings*, Kane, DL, Hinkel, KM (eds). Fairbanks; Vol. 1, 361-366. DOI: 10.13140/2.1.2043.5526

Doran PT, McKay CP, Clow GD, Dana GL, Fountain AG, Nylen T, Lyons WB. 2002. Valley floor climate observations from the McMurdo Dry Valleys, Antarctica, 1986-2000. *Journal of Geophysical Research* **107**: 4774–4784. DOI:10.1029/2001JD002045

Douglas TA, Fortier D, Shur Y, Kanevskiy MZ, Guo L, Cai Y, Bray M. 2011. Biogeochemical and geocryological characteristics of wedge and thermokarst-cave ice in the CRREL Permafrost Tunnel, Alaska. *Permafrost and Periglacial Processes* **22**: 120-128. DOI: 10.1002/ppp.709

Ferreira T, Rasband W. 2012. *ImageJ User Guide*. http://rsb.info.nih.gov/ij/docs/guide/user-

guide.pdf, January 21 2016.

Fisher, DA. 2005. A process to make massive ice in the martian regolith using diffusion and thermal cracking. *Icarus* **179**: 387-397. DOI:10.1016/j.icarus.2005.07.024

Fisher DA, Lacelle D. 2014. A model for co-isotopic signatures of evolving ground ice in the cold dry environment of Earth and Mars. *Icarus* **243**: 454-470. DOI: 10.1016/j.icarus.2014.08.009.

Fisher DA, Lacelle D, Pollard W, Davila A, McKay CP. 2016. Ground surface temperature and humidity, ground temperature cycles and the ice table depths in University Valley, McMurdo Dry Valleys of Antarctica. *Journal of Geophysical Research* **121**: 2069-2084. DOI:10.1002/2016JF004054.

Fortier D, Kanevskiy MZ, Shur Y. 2008. Genesis of reticulate-chaotic cryostructure in permafrost. Proceedings of the 9th International Conference on Permafrost, June 23- July 3, Fairbanks, USA, p. 451-456.

Fountain AG, Nylen TH, Monaghan A, Basagic HJ, Bromwich D. 2009. Snow in the McMurdo Dry Valleys, Antarctica. *International Journal of Climatology* **30**: 633-642. DOI:10.1002/joc.1933

French HM. 1998. An appraisal of cryostratigraphy in North-West Arctic Canada. *Permafrost and Periglacial Processes* **9**: 297-312.

French H, Shur Y. 2010. The principles of cryostratigraphy. *Earth-Science Reviews* **101**: 190-206. DOI: 10.1016/j.earscirev.2010.04.002

Gilbert GL, Kanevskiy M, Murton JB. 2016. Recent advances (2008-2015) in the study of ground ice and cryostratigraphy. *Permafrost and Periglacial Processes* **27**: 377-389. DOI: 10.1002/ppp.1912

Head, KH. 1992. Manual of soil laboratory testing. Volume 1: soil classification and compaction tests. Second edition. Pentech Press, London. 388pp.

Hounsfield, GN. 1973. Computerized transverse axial scanning (tomography): Part 1. Description of system. *British Journal of Radiology* **46**: 1016-1022.

Jackson A, Davila AF, Böhlke JK, Sturchio NC, Sevanthi R, Estrada N, Brundrett M, Lacelle D, McKay CP, Poghosyan A, Pollard W, Zacny K. 2016. Deposition, accumulation, and alteration of Cl^-, NO_3^-, ClO_4^- and ClO_3^- salts in a hyper-arid polar environment: mass balance

and isotopic constraints. *Geochimica etCosmochimica Acta* **182**: 197-215.DOI: 10.1016/j.gca.2016.03.012

Jensen JR. 2000. Remote sensing of the environment: an Earth resource perspective. Prentice Hall Series in Geographic Information Science. Upper Saddle River, New Jersey, USA. 544pp.

Kanevskiy M, Shur Y, Fortier D, Jorgenson MT, Stephani E. 2011. Cryostratigraphy of late Pleistocene syngenetic permafrost (yedoma) in northern Alaska, Itkillik River exposure. *Quaternary Research* **75**: 584-596. DOI: 10.1016/j.yqres.2010.12.003

Kanevskiy M, Shur Y, Jorgenson MT, Ping C-L, Michaelson GJ, Fortier D, Stephani E, Dillon M, Tumskoy V. 2013. Ground ice in the upper permafrost of the Beaufort Sea coast of Alaska. *Cold Regions Science and Technology* **85**: 56-70. DOI: 10.1016/j.coldregions.2012.08.002

Kanevskiy M, Jorgenson T, Shur Y, O'Donnell JA, Harden JW, Zhuang Q, Fortier D. 2014. Cryostratigraphy and permafrost evolution in the lacustrine lowlands of West-Central Alaska. *Permafrost and Periglacial Processes* **25**: 14-34. DOI: 10.1002/ppp.1800

Kawamura T. 1988. Observations of the internal structure of sea ice by X ray computed tomography. *Journal of Geophysical Research* **93**: 2343–2350. DOI:10.1029/JC093iC03p02343.

Kawamura T. 1990. Nondestructive, three-dimensional density measurements of ice core samples by X ray computed tomography. *Journal of Geophysical Research* **95**: 12407–12412. DOI:10.1029/JB095iB08p12407.

Lacelle D, Davila AF, Pollard WH, Andersen D, Heldmann J, Marinova M, McKay CP. 2011. Stability of massive ground ice bodies in University Valley, McMurdo Dry Valleys of Antarctica: Using stable O-H isotope as tracers of sublimation in hyper-arid regions. *Earth and Planetary Science Letters* **301**: 403-411. DOI:10.1016/j.epsl.2010.11.028

Lacelle D, Davila AF, Fisher D, Pollard WH, DeWitt R, Heldmann J, Marinova MM, McKay CP. 2013. Excess ground ice of condensation-diffusion origin in University Valley, McMurdo Dry Valleys of Antarctica: Evidence from isotope geochemistry and numerical modeling. *Geochimica et Cosmochimica Acta* **120**: 280-297.DOI:10.1016/j.gca.2013.06.032

Lacelle D, Lapalme C, Davila AF, Pollard W, Marinova M, Heldmann J, McKay CP. 2016. Solar radiation and air and ground temperature relations in the cold and hyper-arid

Quartermain Mountains, McMurdo Dry Valleys of Antarctica, *Permafrost and Periglacial Processes* **27:** 163-176. DOI: 10.1002/ppp.1859.

Lapalme C, Lacelle D, Davila AF, Pollard W, Fortier D, McKay CP. 2015. Cryostratigraphy of near-surface permafrost in University Valley, McMurdo Dry Valleys of Antarctica. *Proceedings of the 68th Canadian Geotechnical Conference and the 7th Canadian Permafrost Conference*, September 20-23, Quebec, Canada.

Lapalme C, Lacelle D, Pollard W, Fisher D, Alfonso AF, McKay CP. 2017. Distribution and origin of ground ice in University Valley, McMurdo Dry Valleys, Antarctica. *Antarctic Science* **29:** 183-198. DOI:10.1017/S0954102016000572

Lewis AR, Marchant DR, Ashworth AC, Hemming SR, Machlus ML. 2007. Major middle Miocene global climate change: evidence from East Antarctica and the Transantarctic Mountains. *Geological Society of America Bulletin* **119**: 1449-1461.

Lewis AR, Marchant DR, Ashworth AC, Hedenas L, Hemming SR, Johnson JV, Leng J, Machlus ML, Newton AE, Raine JI, Willenbring JK, Williams M, Wolfe AP. 2008. Mid-Miocene cooling and the extinction of tundra in continental Antarctica. *Proceedings of the National Academy of Sciences of the United States of America* **105**: 10676-10680. DOI:10.1073/pnas.0802501105

Mackay JR. 1972. The world of underground ice. *ANNALS of the Association of American Geographers* **62**: 1-22. DOI:10.1111/j.1467-8306.1972.tb00839.x

Marchant DR, Head III JW. 2007. Antarctic dry valleys: Microclimate zonation, variable geomorphic processes, and implications for assessing climate change on Mars. *Icarus* **19**: 187-222. DOI: 10.1016/J.ICARUS.2007.06.018

Marinova MM, Mckay CP, Pollard WH, Heldmann JL, Davila AF, Anderson DT, Jackson WA, Lacelle D, Paulsen G, Zacny K. 2013. Distribution of depth to ice-cemented soils in the high elevation Quartermain Mountains, McMurdo Dry Valleys, Antarctica. *Antarctic Science* **25**: 575-582. DOI:10.1017/S095410201200123X

McKay CP. 2009. Snow recurrence sets the depth of dry permafrost at high elevations in the McMurdo Dry Valleys of Antarctica. *Antarctic Science* **21**: 89-94. DOI:10.1017/S0954102008001508

Mellon MT. 1997. Small-scale polygonal features on Mars: seasonal thermal contraction cracks in permafrost. *Journal of Geophysical Research – Planets* **102**: 25617-25628. DOI:10.1029/97JE02582

Mellon MT, McKay CP, Heldmann JL. 2014. Polygonal ground in the McMurdo Dry Valleys of Antarctica and its relationship to ice-table depth and the recent Antarctic climate history. Antarctic Science 26: 413-426. DOI:10.1017/S0954102013000710

Murton JB, French HM. 1994. Cryostructures in permafrost, Tuktoyaktuk coastlands, western arctic Canada. *Canadian Journal of Earth Sciences* **31**: 737-747. DOI: 10.1139/e94-067

Obbard RW, Troderman G, Baker I. 2009. Correspondence: Imaging brine and air inclusions in sea ice using micro-X-ray computed tomography. *Journal of Glaciology* **55:** 1113-1115. DOI:10.5194/acpd-15-13167-2015

O'Neil BH, Burn CR. 2012. Physical and temporal factors controlling the development of near-surface ground ice at Illisarvik, western Arctic coast, Canada. *Canadian Journal of Earth Sciences* **49**: 1096-1110. DOI:10.1139/e2012-043

Pollard WH, Lacelle D, Davila AF, Andersen D, Mckay CP, Marinova M, Heldmann J. 2012. Ground ice conditions in University Valley, McMurdo Dry Valleys, Antarctica. *Proceedings of the 10th International Conference on Permafrost*, June 25-29, Salekhard, Russia, Hinkel KM (ed). Vol. 1: 305–310.

Sizemore HG, Mellon MT. 2008. Laboratory characterization of the structural properties controlling dynamical gas transport in Mars-analog soils. *Icarus* **197:** 606-620. DOI: 10.1016/j.icarus.2008.05.013

Shur Y, French HM, Bray MT, Anderson DA. 2004. Syngenetic permafrost growth: cryostratigraphic observations from the CRREL tunnel near Fairbanks, Alaska. *Permafrost and Periglacial Processes* **15**: 339-347. DOI:10.1002/ppp.486

Stephani E, Fortier D, Shur Y. 2010. A cryofacies approach to describe ground ice in permafrost for engineering applications – Case study of a road test site on the Alaska Highway (Beaver Creek, Yukon, Canada). *Proceedings of the 63rd Canadian Geotechnical Conference and the 6th Canadian Permafrost Conference, September 12-16, Calgary, Canada*, 476-483. DOI:10.13140/2.1.2467.2961.

Trinh-Le CA. 2017. Dry sedimentation processes in the high-elevation McMurdo Dry Valleys, Antarctica: A case study in University Valley. Master's thesis, Victoria University of

Wellington, Wellington, New Zealand. Retrieved from.

Torrance JK, Elliot T, Martin R, Heck RJ. 2008. X-ray computed tomography of frozen soil. *Cold Regions Science and Technology* **53**: 75-82. DOI:10.1016/j.coldregions.2007.04.010

van Everdingen R. (ed.). 1998. *Multi-language glossary of permafrost and related ground-ice terms*. National Snow and Ice Data Center/World Data Center for Glaciology: Boulder, Colorado.

Figure Captions

Figure 1a. Hillshade image showing the location of University Valley (black rectangle) in the Quartermain Mountains of the McMurdo Dry Valleys. The inset map shows the location of the McMurdo Dry Valleys in Antarctica; **b.** Hillshade image showing the location of core sampling sites within University Valley; **c.** Photograph illustrating the location of "University Glacier" and a down-valley view of University Valley; **d.** Photograph illustrating snow in the troughs of sand-wedge polygons in University Valley; **e.** Map showing the ground surface temperature zones in University Valley and the location of the four polygons analyzed in this study (from Lacelle *et al.,* 2016). The hillshades were derived from a LiDAR digital elevation model (http://usarc.usgs.gov/lida_dload.shtml) embedded into a 15 m ASTER digital elevation model of the upper McMurdo Dry Valleys (http://asterweb.jpl.nasa.gov/data/asp). The contours (white lines) on a, b and e are at 100 m intervals.

Figure 2a. Grain-size distribution (%) of cores P8-C6, P8-C3, P1-C1, P7-C1 and P6-C5 with depth; the location of the permafrost table and the ice table is indicated for each core; **b.** Ternary plot showing the particle-size distribution of the five permafrost cores collected in University Valley. Gravel (≥2 mm), sand (<2 mm to ≥0.0625 mm) and fine (<0.0625 mm) sediments; **c.** Pore size diameter (μm) and cumulative distribution (%) in two representative samples of P8-C3 and P1-C1.

Figure 3. Examples of the **a.** structureless, **b.** porous visible, **c.** crustal and **d.** suspended cryostructures observed in the binary images of the five permafrost cores collected in University Valley. The black tones in the thresholded (-320 to 775 HU) images on the right represent ground ice and white tones represent all other components; the images on the left represent the scan image with enhanced brightness and contrast. Images are oriented so that the top of the core points upward.

Figure 4. Reconstructions of the CT scan images of vertical sections through cores P8-C3 (42.5 cm long), P8-C6 (40 cm), P7-C1 (27 cm), P6-C5 (71.5 cm) and P1-C1 (70 cm). **i.** Contrast and brightness adjusted view of core. **ii.** Ice threshold (–320 to 775 HU) applied to core. The darker tones in each image represent ice. The top of each core is at the top of its respective image.

Figure 5. Ice contents and cryostructure distribution of permafrost cores P8-C3 (a), P8-C6 (b), P6-C5 (c), P1-C1 (d) and P7-C1 (e) from University Valley. **i.** Amount and distribution of measured excess ice content (EIC) and volumetric ice content (VIC) compared to volumetric ice content derived from the stack of -320 to 775 HU thresholded images (VIC_{CT}). Cryofacies type divisions are also indicated; **ii.** Distribution of suspended, structureless, crustal and porous visible cryostructures. The designation of a cryofacies type at specific depths within the cores depended on the method used to derive volumetric ice content (i.e. VIC or VIC_{CT}). The black rectangle in **ai.** indicates an imaging error in the stack of CT scan images.

Figure 6a. Relation between measured volumetric ice content (VIC) in the five permafrost cores and VIC_{CT} averaged over the same depth interval; **b.** Relation between excess ice content (EIC) measured in the five permafrost cores and VIC_{CT} averaged over the same depth interval.

Figure 7. Apparent ice accumulation rates for three cores discussed in this paper (P8-C3, P6-C5 and P1-C1) and three cores discussed in Lapalme *et al.* (2017) (P12, P1-C2 and P6-C3) located in the perennially cryotic zone and seasonally non-cryotic zone. The two cores taken from the intermediate mixed zone (P6-C3 and P6-C5) are grouped in the perennially cryotic zone as their ground ice originated from vapour deposition. Accumulation rates from a drained lake basin and hummocky terrain in northwest Canada (O'Neil and Burn, 2012; and reference therein) have been added for comparison.

Figure 8. Schematic diagram illustrating the transition, through time, from dry sediment to icy permafrost in University Valley. The sketch depicts a dry sand that is subsequently filled with pore ice and then subjected to thermal and elastic stresses. This results in an increase of the available pore space, which then becomes partially filled with new ice (either from vapour deposition or infiltration of partially evaporated snow meltwater).

Figure 9. Schematic diagram illustrating a permafrost column with a dry soil layer between the permafrost table and the ice table, typical of soils in the upper McMurdo Dry Valleys of

Antarctica. The depth at which a paleo-sublimation unconformity may be observed is also indicated.

Table 1. Details of the five ice-bearing permafrost cores collected from University Valley, McMurdo Dry Valleys of Antarctica.

Core ID	Latitude (South)	Longitude (East)	Ice table depth (cm)	Length of core collected in field (cm)	Length of core analyzed by CT scan (cm)	Ground temperature zone	Surficial sediments
13-P8-C3	77.86563	160.72627	2	68	42.5	PCZ	Colluvium
13-P8-C6	77.86563	160.72627	2	40	40	PCZ	Colluvium
13-P7-C1	77.86422	160.72297	22	27	27	NCZ	Alpine drift
13-P6-C5	77.86341	160.72222	20	71.5	71.5	IMZ	Alpine drift
13-P1-C1	77.86508	160.70158	30	107	70	NCZ	Alpine drift

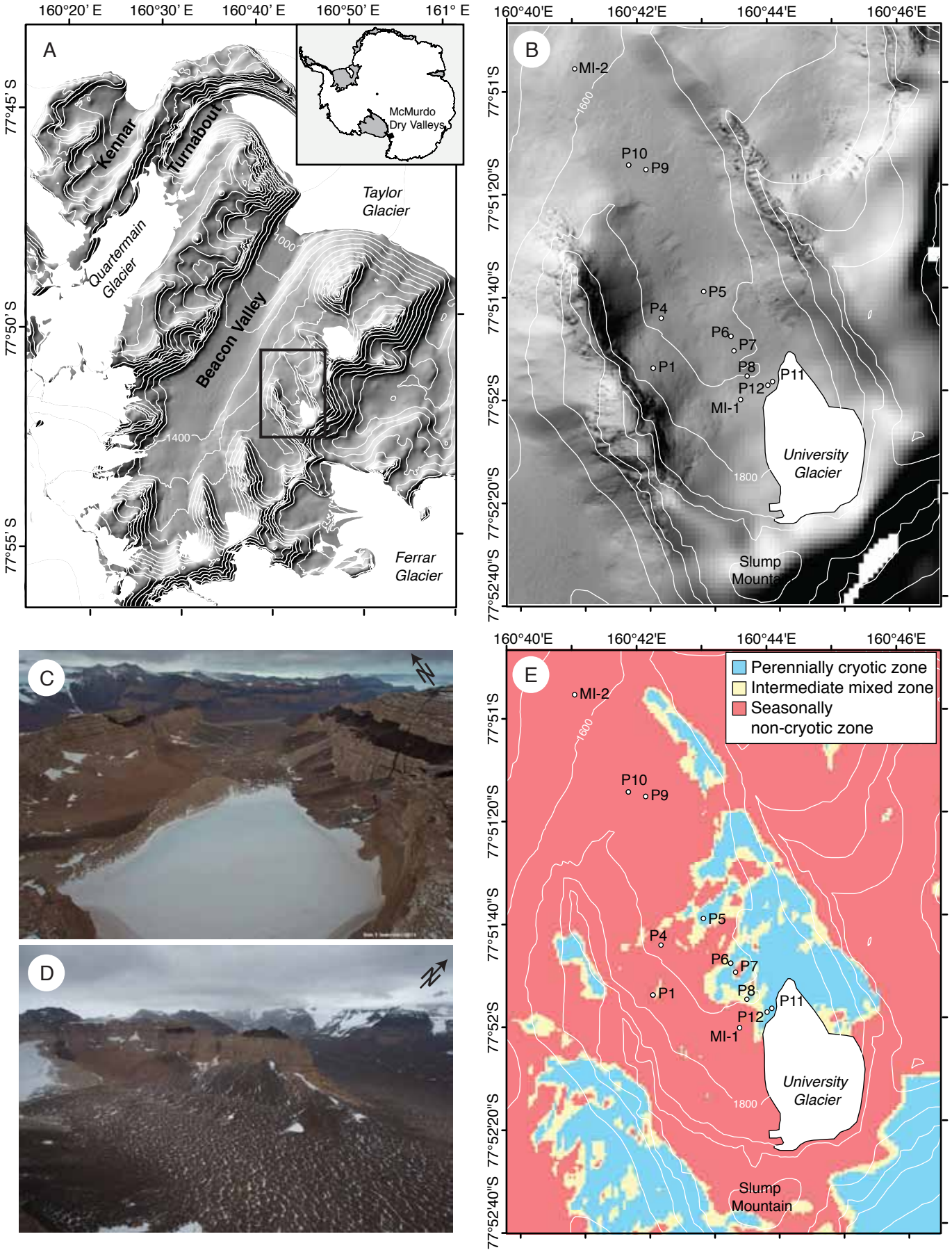
A
160°20' E
160°30' E
160°40' E
160°50' E
161° E
77°45' S
77°50' S
77°55' S
Kennar
Turnabout
Taylor Glacier
Quartermain Glacier
Beacon Valley
Ferrar Glacier
1000
1400
McMurdo Dry Valleys
B
160°40'E
160°42'E
160°44'E
160°46'E
77°51'S
77°51'20"S
77°51'40"S
77°52'S
77°52'20"S
77°52'40"S
MI-2
1600
P10
P9
P5
P4
P6
P7
P1
P8
P11
P12
MI-1
University Glacier
1800
Slump Mountain
C
N
D
N
E
Perennially cryotic zone
Intermediate mixed zone
Seasonally non-cryotic zone
MI-2
1600
P10
P9
P5
P4
P6
P7
P1
P8
P11
P12
MI-1
University Glacier
1800
Slump Mountain

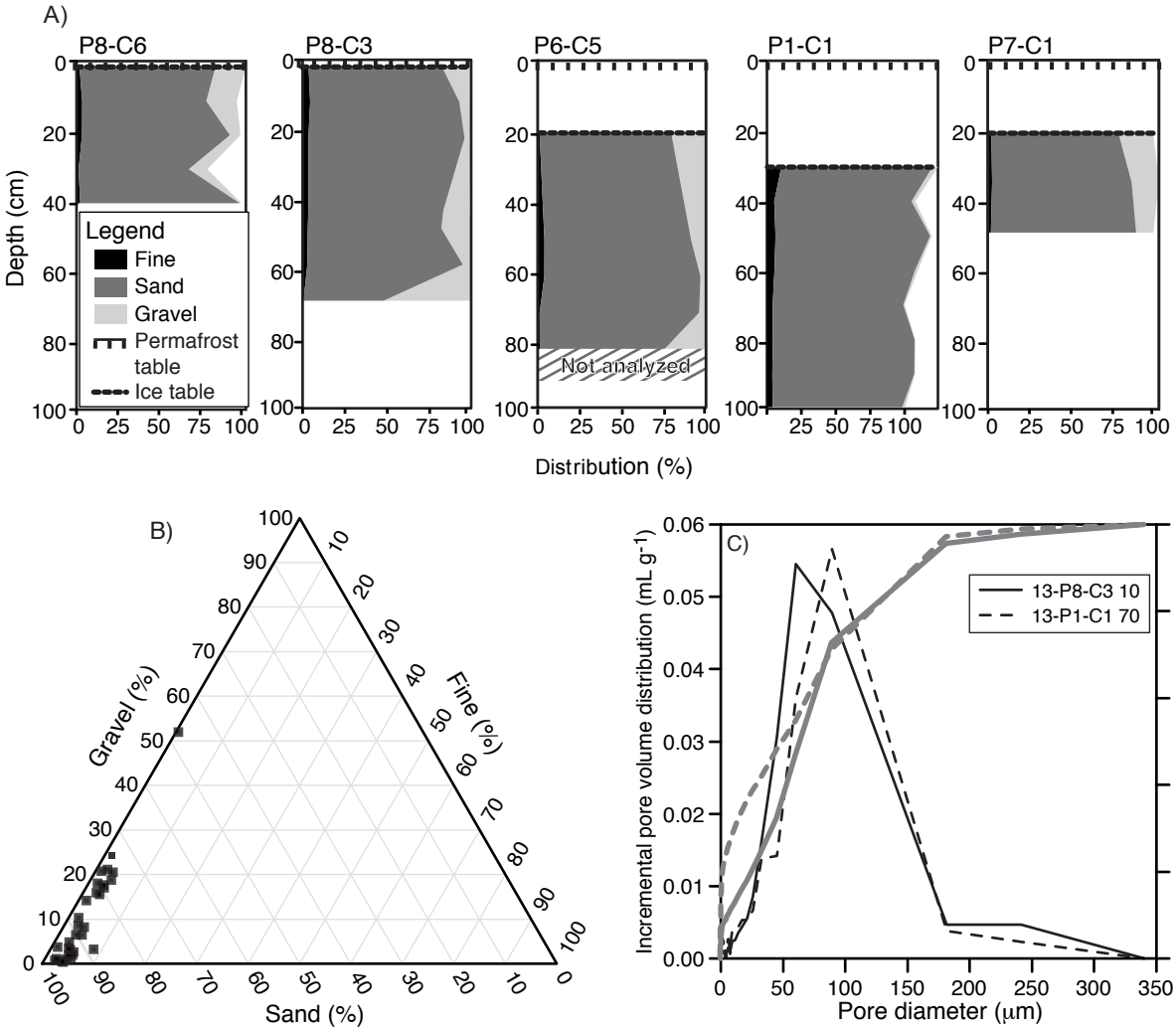
A)
P8-C6
P8-C3
P6-C5
P1-C1
P7-C1
Depth (cm)
Legend
Fine
Sand
Gravel
Permafrost table
Ice table
Not analyzed
Distribution (%)
B)
Gravel (%)
Fine (%)
Sand (%)
C)
13-P8-C3 10
13-P1-C1 70
Incremental pore volume distribution (mL g-1)
Cumulative distribution (%)
Pore diameter (μm)

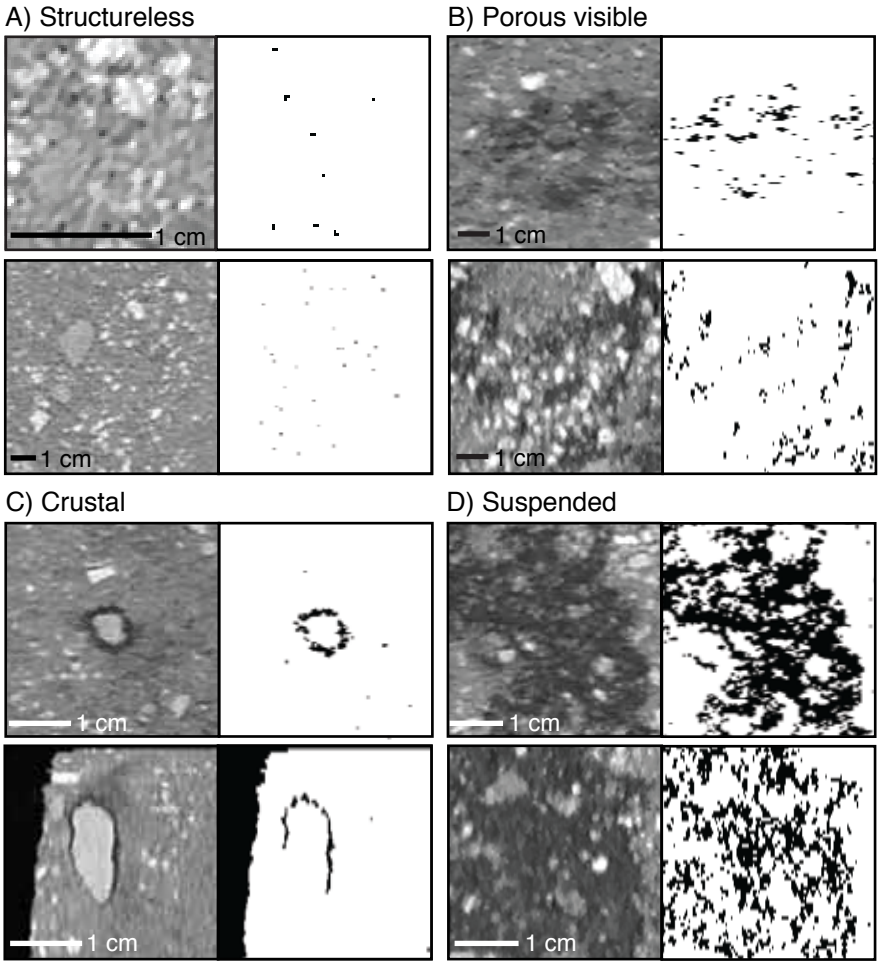
A) Structureless
B) Porous visible
C) Crustal
D) Suspended
1 cm
1 cm
1 cm
1 cm
1 cm
1 cm
1 cm
1 cm


P8-C3
(i)
(ii)
P6-C5
(i)
(ii)
P1-C1
(i)
(ii)
P8-C6
(i)
(ii)
P7-C1
(i)
(ii)
2 cm

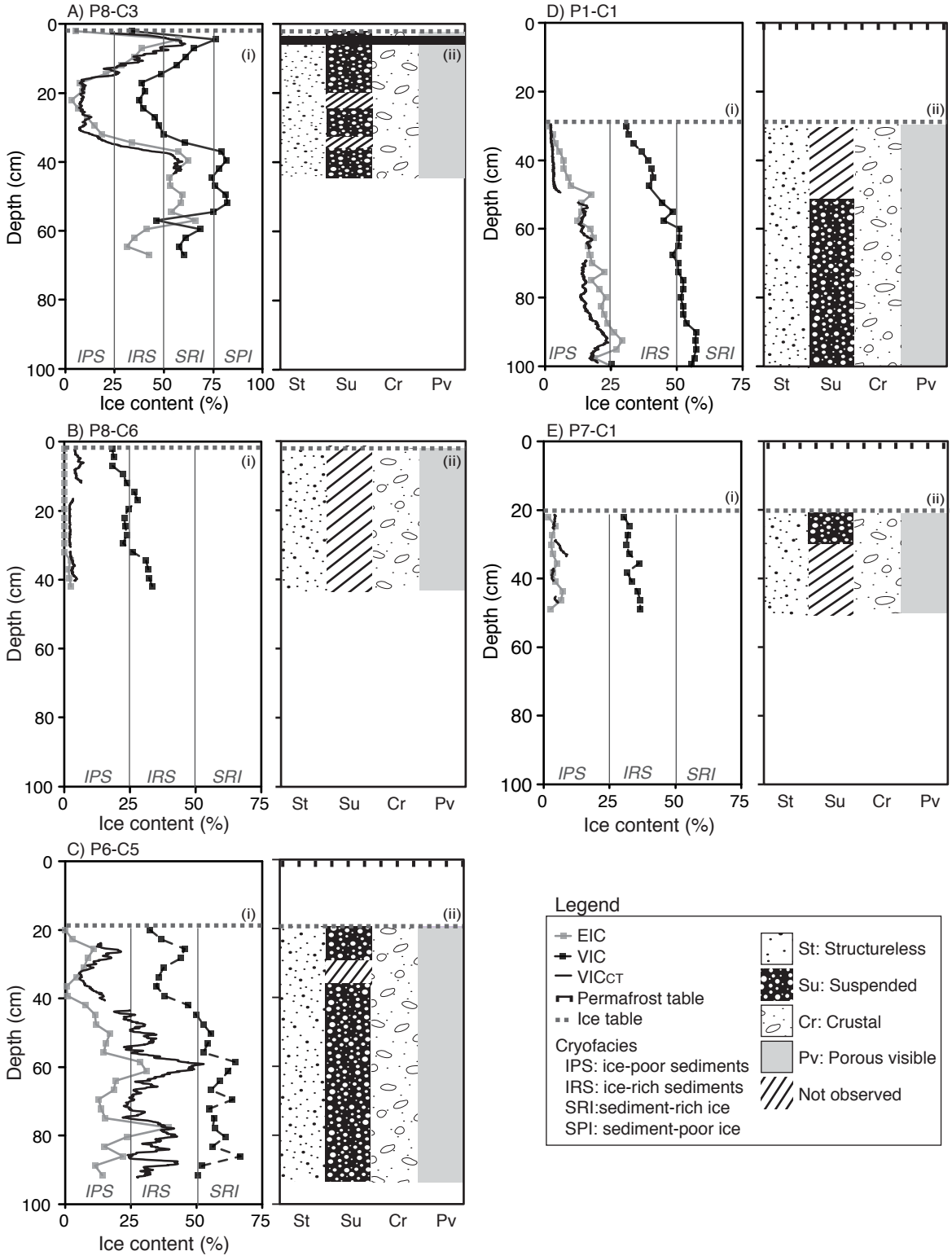
A) P8-C3
B) P8-C6
C) P6-C5
D) P1-C1
E) P7-C1
Depth (cm)
Ice content (%)
IPS
IRS
SRI
SPI
(i)
(ii)
St
Su
Cr
Pv
Legend
EIC
VIC
VICCT
Permafrost table
Ice table
Cryofacies
IPS: ice-poor sediments
IRS: ice-rich sediments
SRI:sediment-rich ice
SPI: sediment-poor ice
St: Structureless
Su: Suspended
Cr: Crustal
Pv: Porous visible
Not observed

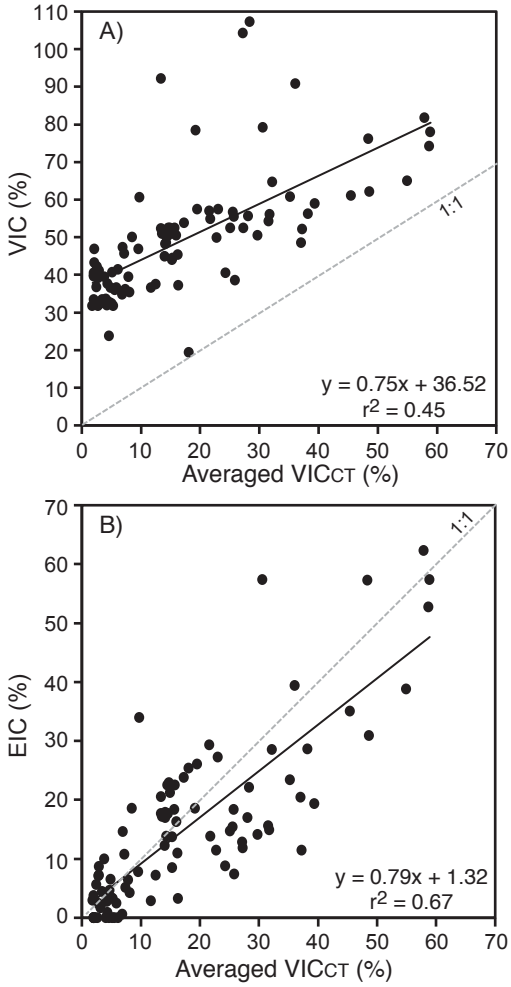
A)
VIC (%)
Averaged VICCT (%)
1:1
y = 0.75x + 36.52
r2 = 0.45
B)
EIC (%)
Averaged VICCT (%)
1:1
y = 0.79x + 1.32
r2 = 0.67

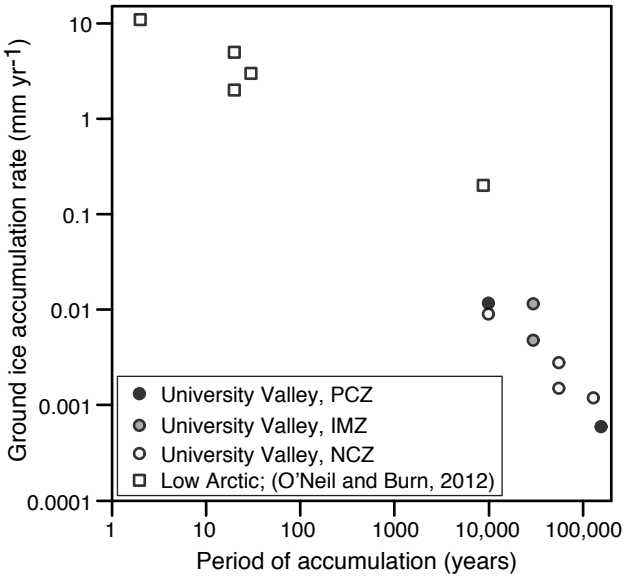
Ground ice accumulation rate (mm yr-1)
10
1
0.1
0.01
0.001
0.0001
1
10
100
1000
10,000
100,000
Period of accumulation (years)
University Valley, PCZ
University Valley, IMZ
University Valley, NCZ
Low Arctic; (O'Neil and Burn, 2012)

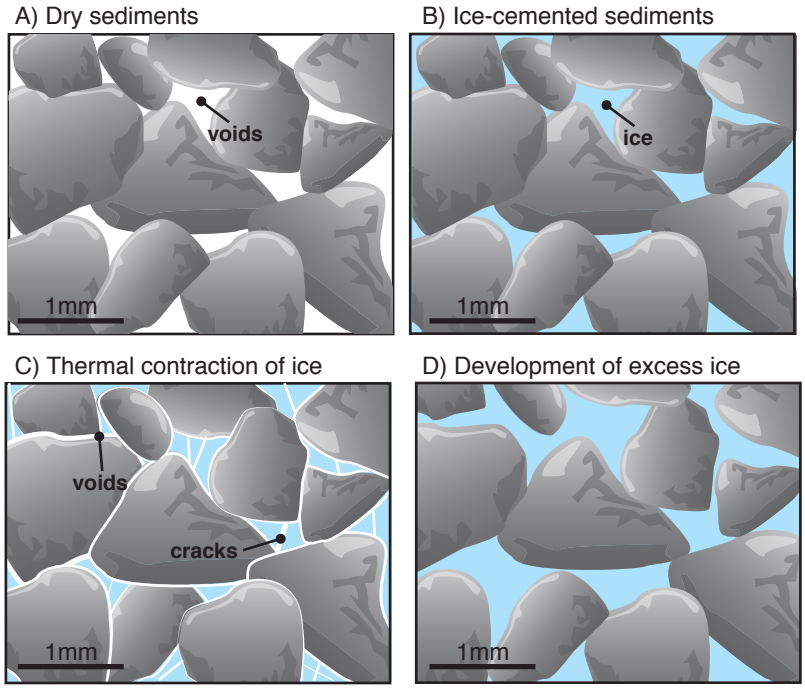
A) Dry sediments
voids
1mm
B) Ice-cemented sediments
ice
1mm
C) Thermal contraction of ice
voids
cracks
1mm
D) Development of excess ice
1mm

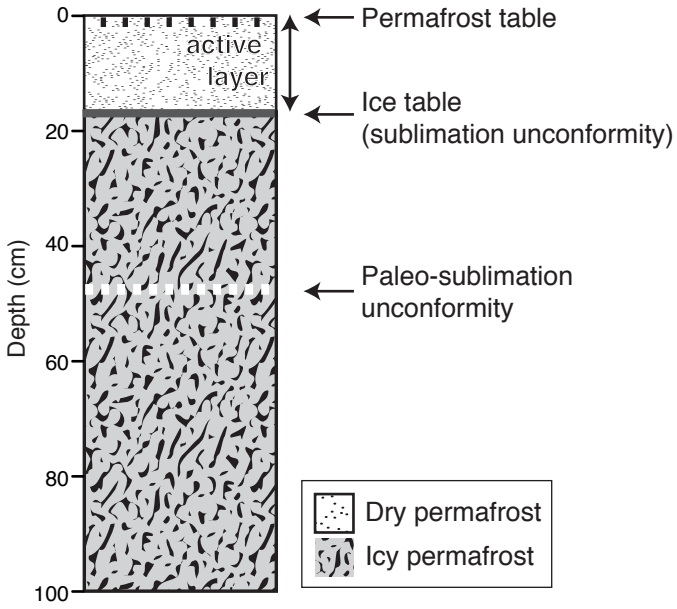
0
20
40
60
80
100
Depth (cm)
active layer
Permafrost table
Ice table
(sublimation unconformity)
Paleo-sublimation
unconformity
Dry permafrost
Icy permafrost